Mechanical Design of the Multirotor Test Bed

Sarah Conley
sarah.a.conley@nasa.gov
Mechanical Engineer
NASA Ames Research Center
Moffett Field, CA, USA

Carl Russell
carl.r.russell@nasa.gov
Aerospace Engineer
NASA Ames Research Center
Moffett Field, CA, USA

ABSTRACT

The Multirotor Test Bed (MTB) is a new capability for testing a wide array of advanced vertical take-off and landing (VTOL) rotor configurations, with a primary focus on testing in the U.S. Army's 7-by 10-Foot Wind Tunnel at NASA Ames Research Center. The MTB was designed to allow adjustment of the vertical, lateral, and longitudinal placement of each rotor, as well as allow tilt adjustment of each rotor and pitch adjustment of the whole assembly. Each rotor can tilt forward 90 deg and backwards 5 deg. In addition, the entire MTB is able to tilt forward 20 deg and backwards 10 deg. This flexibility allows for the system to be tested in many different configurations. There is a six-axis load cell under each rotor assembly, to measure the loads and vibrations produced by each rotor. The wind tunnel scales are used to measure loads on the full assembly. Phased microphone arrays were placed in the wall and ceiling of the wind tunnel test section to obtain acoustic data for the rotors in different configurations. The loads and acoustic data will be used to validate existing computational models as well as to evaluate the performance of new multirotor aircraft systems. The overall goal of the MTB project is to help gain a better understanding of the performance, control, interactional aerodynamics, and acoustics of multirotor systems of this size. This paper describes the mechanical design of the MTB and presents an overview of the analyses used to ensure the MTB would be able to safely operate in the wind tunnel as well as yield accurate measurements.

INTRODUCTION

Advanced multirotor vertical flight aircraft concepts are emerging faster than rigorous individualized tests can investigate their utility and performance. Additionally, rotorcraft operate in a challenging environment of extremely complex aerodynamics that are difficult to accurately simulate with computational fluid dynamics (CFD). Wind tunnel testing serves a critical role in providing validation data to help improve rotor performance predictions, but wind tunnel test data for multirotor systems have only recently started to become available.

Two previous NASA wind tunnel tests of multirotor UAS vehicles were conducted in October-December 2015 [Ref. 1] and January-February 2017 [Ref. 2 and 3]– referred to as the MUAS1 and MUAS2 tests, respectively. The MUAS (Multicopter Unmanned Aerial System) tests measured the aerodynamic performance of five quadcopters (3DR SOLO, 3DR Iris+, DJI Phantom 3 Advanced, SUI Endurance, and the ARL Overlapped Quadrotor), a tilt-wing (Elytron 4S UAV), and an octocopter (Drone America x8). The MUAS1 test entry generated a high-quality set of performance data for these vehicles, but it also raised additional questions, particularly related to vibrations, blade deflections, aerodynamic interference, acoustics, and trim strategies. The MUAS2 test expanded on the first test series by attempting to better characterize vibrations, interactional aerodynamics, and blade motion.

The MUAS tests had three main limitations:

- Loads were only measured for the entire vehicle, so a full picture of interactional aerodynamics could not be gleaned from the data.
- Testing was limited to existing vehicles with no ability to alter the configuration.
- Testing focused on small UAS vehicles, with blade Reynolds numbers below 100,000 – a regime with different rotor performance characteristics than those seen in typical Urban Air Mobility (UAM) applications.

The Multirotor Test Bed (MTB) program builds upon the knowledge and capabilities developed during the MUAS tests. By measuring individual rotor loads for a multirotor system and allowing for adjustments to rotor position and attitude, the MTB will provide a wealth of data on the aeromechanics of arbitrary multirotor configurations. The adjustment capabilities of the MTB will allow the multirotor design space to be parametrically explored and optimized. The MTB is also at a larger scale than the small unmanned aerial systems (UAS) that have been tested before, which will allow for testing at Reynolds numbers more relevant to full-scale piloted electric vertical take-off and landing (eVTOL) aircraft. The full-scale model of the MTB in the U.S. Army's 7-by 10-Foot Wind Tunnel is shown in Figure 1.

Presented at the VFS Aeromechanics for Advanced Vertical Flight Technical Meeting, San Jose, CA, January 21–23, 2020.

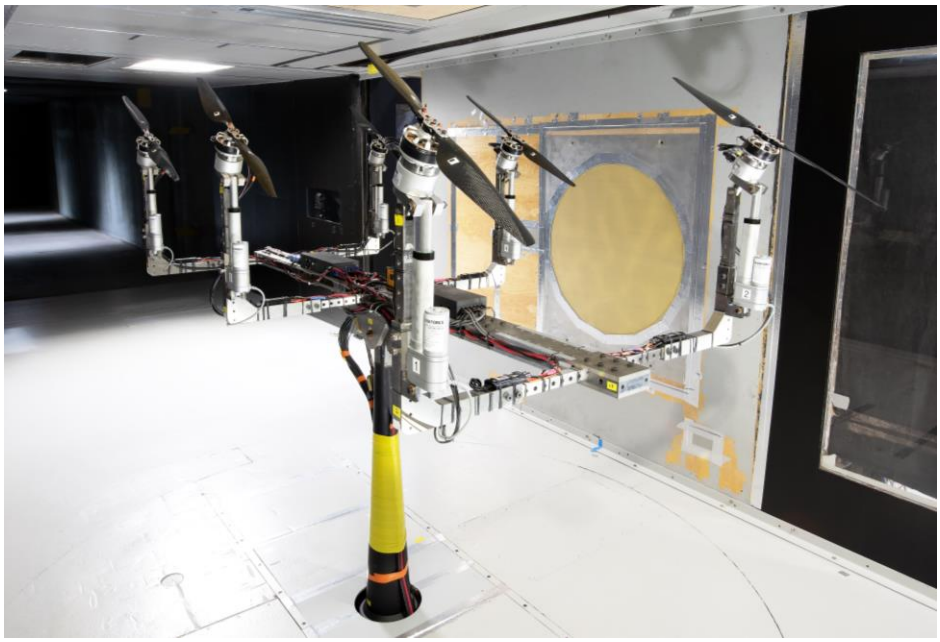

Figure 1: MTB in 7-by 10-Foot Wind Tunnel.

Many rotorcraft concepts with 6 (or more) rotors have been proposed by a number of different eVTOL companies, but significant testing still needs to be done to evaluate key parameters including performance, safety, and comfort for human passengers. In addition to allowing for the evaluation of fundamental rotor-rotor interactions, the test capabilities of the MTB will be available for future tests of new multirotor aircraft concepts or rotor configurations. Such ability will aid in risk-reduction activities for organizations developing advanced eVTOL aircraft before committing to the expense and complexity of moving on to full-scale testing.

DESIGN

Overview

The Multirotor Test Bed consists of six individual rotor assemblies, each with its own lateral, vertical, and tilt adjustment systems. For the initial testing configuration, each rotor is 24.5 inches in diameter and can pitch forward 90 deg and backwards 5 deg. Smaller rotors can be installed, but the ~2-ft diameter of the baseline configuration is the practical upper limit on rotor size for the MTB. The central support of the design is the strongback, which acts as a structural backbone for the assembly. Lateral support beams are held in the strongback and connect to the adjusting L-brackets. The rotor assemblies are connected to the vertical support beams. The tilt system for each rotor uses a linear actuator which is controlled remotely during testing. The pitch adjustment for the strongback is controlled by a stepper motor interfacing with a jackscrew within the strut that supports the MTB in the wind tunnel. The whole assembly can pitch 20 deg forward (nose down) and 10 deg backward (nose up). There are load cells under each rotor to capture loads and vibrations. A CAD model of the Top Assembly is shown in Figure 2.

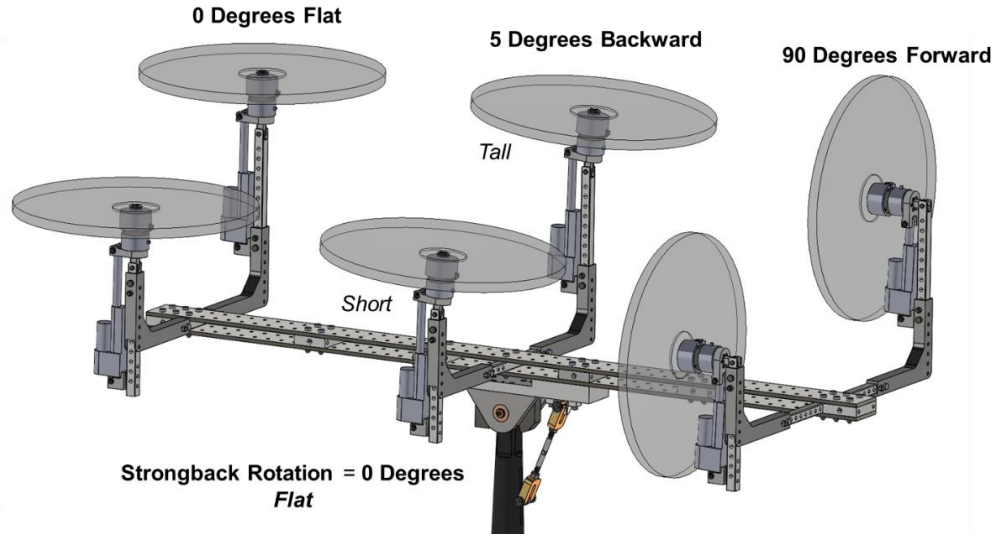

Figure 2: MTB, side view of assembly.

The total weight of the assembly is about 247 lb, not including the strut, which weighs approximately 340 lb. The maximum dimensions of the MTB are 80.63 inches long by 62.45 inches wide by 33.625 inches tall (not including the strut). The MTB was tested in the U.S. Army's 7-by 10-Foot Wind Tunnel at NASA Ames Research Center during fall of 2019. The MTB was designed to be able to withstand all planned testing conditions (with considerable margin) in the 7-by 10-Foot Wind Tunnel, as well as be able to take accurate measurements. The data from the first tunnel entry is currently being processed, and an overview of the test and data will be presented in Refs. 4 and 5.

Other than the off the shelf parts, all custom manufactured parts were constructed from the four materials listed in Table 1.

Table 1: List of Materials used on MTB.

Material	Ultimate Strength (ksi)	Yield Strength (ksi)
AISI 4130 Steel	180	160
17-4PH H900	200	185
13-8PH H950	220	205
932 Bearing Bronze	35	20

For a complete list of properties of each material, see Tables 3 through 6 in the Appendix.

Strongback Assembly

The strongback assembly was designed for high strength and adjustability. The strongback is comprised of a top and bottom plate, center support blocks, and shoulder bolts (see Figure 3). The lateral support beams can slide along the top and bottom plates and are fixed in place by fitting shoulder bolts through the holes. The center support blocks hold the top and bottom plates together, stiffening the strongback assembly. Locknuts are screwed onto the shoulder bolts, ensuring that they will not back out from vibrations. 17-4PH H900 was chosen as the material to meet stiffness requirements. As shown in the loads and analysis section, the safety factors are quite high. The driving design consideration was to provide high precision measurements during testing, which is what determined the stiffness requirement.

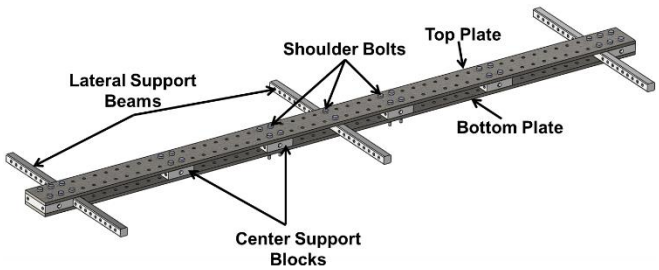

Figure 3: Isometric view of strongback.

The strongback plates are 4 inches wide and 3/8 inches thick, with two rows of holes to securely fix the positions of the lateral support beams. It should be noted that if the strongback has a resonant frequency at a rotor speed that is required for testing, the support blocks can be moved, or additional blocks can be added or removed from the strongback to modify the natural frequencies of the assembly.

Strut Assembly

Going from top to bottom, the strut assembly consists of: the strongback – support interface, large hinges, a shaft, strut washers, strut washer interfaces, hard stops, the strut, a designed lug, screws, dowel pins, the top clevis, locknuts, a threaded rod, the bottom clevis, shaft collars, and a lug (ear). A view of the CAD model of the MTB Strut Assembly is shown in Figure 4.

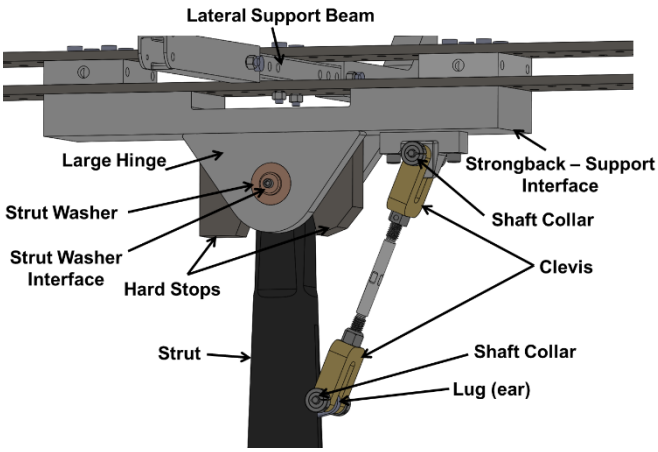

Figure 4: View of Strut Assembly.

Inside the strut is a built-in jackscrew that moves the lug (ear) up and down. The strut was manufactured for previous 7-by 10-ft Wind Tunnel testing and was repurposed for the MTB project. The strut was secured to the turntable on the balance frame of the wind tunnel, which is supported by the tunnel scale system for measuring loads on the entire assembly (described more in the Installation Assembly section).

The strongback-support interface supports the strongback assembly. Shoulder bolts go through the strongback assembly, through support blocks, and tap into the strongback-support interface. There are more holes in the strongback-support interface than are needed for the support blocks. The purpose of the extra holes is to allow the positioning of the support blocks and shoulder bolts in three different configurations. This was done in case a different configuration was desired in which the beam assemblies were moved closer to the center of the strongback.

The large hinges and strut washers allow the entire assembly to rotate on the shaft which goes through the top of the single heavy strut. The strut washers act as bearings and are press fit into the large hinges. The shaft has a slip fit with the strut washers. The shaft is tapped on each end and is secured in place by the strut washer interfaces and screws on either side. The intent of this design is to reduce friction along the shaft as well as take away any slop between the strut and the hinge. Originally the strut assembly was manufactured with high-load ball bearings that had some mechanical play, and there was a smaller contact surface between the strut and

the hinge. As a result, there was significant lateral movement of the entire strongback. Thus, strut washers were created to have more surface contact between the strut and the hinge, as well as take away any additional slop or movement that was allowed by the ball bearings. This solution eliminated the sideways movement. Countersunk shoulder bolts secure the large hinges to the strongback-support interface and a dowel pin was pressfit into the hinge to ensure the hinge was positioned correctly on the strongback-support interface.

Similar to the large hinges, the hard stops are secured to the strongback-support interface via shoulder bolts, which are countersunk into the interface and tap into the hard stops. There is an upstream (left, in Fig. 5) and downstream (right) hard stop. The purpose of the hard stops is to prevent the MTB from damaging the wind tunnel in the event of a mechanical failure of the threaded rod or adjacent parts. If the rotating mechanism fails or becomes disconnected, the MTB will rotate forward or backward on the strut depending on the configuration of the rotors. The hard stops will prevent the MTB from rotating past the point where it hits the floor or ceiling of the wind tunnel. It should be noted that when the back two rotors are in their tallest position, they are capable of hitting the ceiling of the tunnel when the MTB is pitched more than 22 deg forward. The tallest safe operating condition for the back two rotors is when they are in their third tallest position. All other rotors can be in any configuration and not hit the floor or ceiling of the tunnel.

The designed lug (see Figure 5) screws into the bottom of the strongback-support interface. A swivel joint (not shown) is press fit into the designed lug. Flanged bearings are press fit into the top clevis, and the dowel pin has a slip fit with the flanged bearings and the swivel joint. Thus, the top clevis can rotate about the dowel pin that goes through the designed lug, and the dowel is held in place with shaft collars on either side.

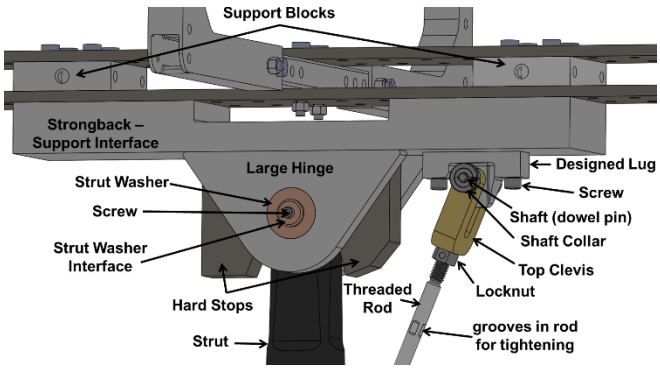

Figure 5: Close up view of top of strut assembly.

The top clevis is connected to the bottom clevis by a threaded rod. All parts described up to now, excluding off the shelf parts, are made from 17-4 except for the clevises, which are made from AISI 4130. The threaded rod is threaded on both ends in different directions (right-hand and left-hand threads). When the threaded rod is turned one way it will screw into both the top and bottom clevis, and when it turns the other way, it will screw out of the clevises. This was done for ease of assembly, as well as to allow for additional adjustment of the strongback pitch angle. The threaded rod has machined flat spots in the center, so a wrench can easily turn it.

The clevises are tapped and there are locknuts that secure the position of the threaded rod with respect to the points of rotation and prevent backout. The distance between the points of rotation was optimized to get the maximum amount of rotation for the assembly. The placement of the designed lug was also part of this optimization. The operational range of motion of the MTB is currently 20 deg forward and 10 deg backward, but the maximum range of motion could be extended to 32.5 deg forward and 13.6 deg backward.

Flanged bearings are also press fit into the bottom clevis. A dowel pin has a slip fit into these bearings and through the lug (which is part of the single heavy strut) and is held in place via shaft collars. Additional thrust bearings are placed between the clevis and the lug so the clevis can rotate freely along the dowel pin.

Beam System

The beam system consists of the lateral support beam, vertical support beam, adjusting L-brackets, shoulder bolts, and locknuts. The lateral support beam is fixed to the strongback, in the middle, in between the top and bottom strongback plates, via two shoulder bolts (see Figure 6). There are two adjusting L-brackets on either side of the lateral support beam. The adjusting L-brackets have two through holes on the horizontal side and on the vertical side and slide along the fixed lateral support beam and the vertical support beam, respectively.

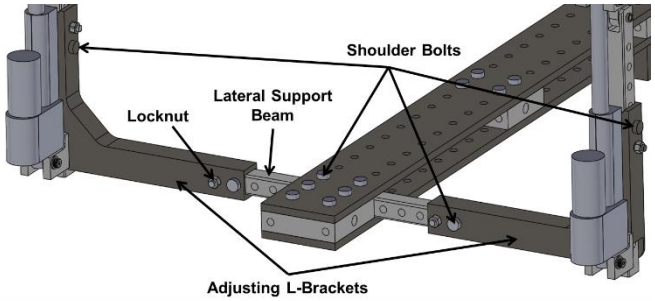

Figure 6: Isometric view of lateral beam system.

To change the lateral position of the rotor, the shoulder bolts and locknuts are removed, the adjusting L-bracket is manually moved to the desired location, and it is secured in that location with the shoulder bolts and locknuts. The gap between the rotors is smallest when the adjusting L-brackets are fixed closest to the strongback (see Figure 7), and the gap is the largest when the adjusting L-brackets are fixed to the farthest holes on the lateral support beam (see Figure 8). The current model has 24.5 inch diameter rotors, which gives a small gap of 0.2 inches (Figure 7) and a large gap of 14.2 inches (Figure 8).

Figure 7: Front view of small gap, with 24.5 inch diameter rotors.

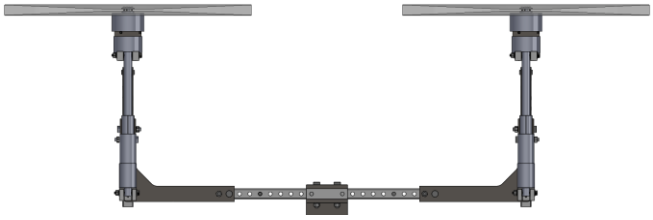

Figure 8: Front view of large gap, with 24 inch diameter rotors.

After analysis, it was determined that the adjusting L-brackets would be made out of 17-4PH H900 Stainless Steel and the support beams would be made out of 13-8PH H950 Stainless Steel. It is essential that this assembly is very stiff and deflection is minimal in order to obtain accurate measurements. Additionally, the thickness of the adjusting L-bracket was increased along the vertical side to improve stiffness. The adjusting L-brackets and the support beams were made of different materials to eliminate the possibility of galling.

There is a slip fit in between the adjusting L-brackets and the support beams. The tolerance on these parts is very small because the slip fit must be retained at temperatures ranging from 35℉ to 105℉. In order to create this fit, the cut outs in the adjusting L-brackets were made through wire electrical discharge machining (EDM). The vertical and lateral support beams were also machined and ground down to a tight tolerance.

There are plans for other lateral support beams to be manufactured in the future with the same design, just modifying the length. If there were multiple lateral support beams, the larger gap could be extended, and the MTB would be capable of being tested in even more configurations.

To adjust the height of the rotor, the vertical support beam moves up and down inside the adjusting L-bracket. When the shoulder bolts and locknuts are removed, the vertical support is manually moved to the desired location, and the shoulder bolts are placed in the holes and secured to that location via the locknuts.

There are three mounting holes for the bottom clevis (see Figure 9 and 11) in the vertical support beam even though the bottom clevis only requires two holes. The additional hole is needed to be able to reach the targeted 10 deg backward position. The range of motion of the linear actuator (the stroke length) was expected to be 3.94 inches as described by the manufacturer. However, after obtaining the linear actuator and testing it, the actual range of motion was only 3.75 inches. For this reason, the extra hole was added into the vertical support beam. When the clevis is secured to the two bottom holes, the range of motion is 90 deg forward (airplane mode) and 5 deg backward. When the clevis is secured to the two top holes, the range of motion is 62 deg forward and 20 deg backward. The linear actuator is restricted from going backwards because it interferes with the adjusting L-bracket. The overall maximum range is 20 deg backward, but the safe operational range is 15 deg backward when the clevis is secured to the top two holes in the vertical support beam. At 15 deg backwards, the minimum gap between the linear actuator and the adjusting L-bracket is 0.11 inches.

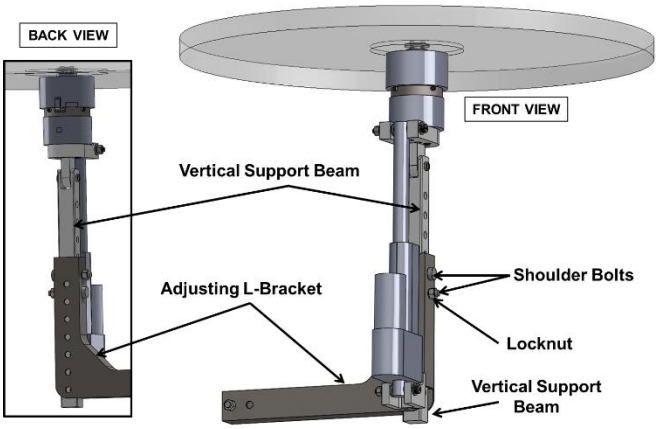

Figure 9: Front (right) and back (left) view of vertical beam system in medium height configuration.

The minimum and maximum height of the vertical beam assembly above the strongback is approximately 13 inches and 22 inches (see Figure 10) with a range of 9 inches and increments of 1 inch. It should be noted that the safety mechanisms (the stoppers) used to prevent the rotors from hitting the walls (including ceiling and floor) of the wind tunnel, were designed using the current dimensions of the beam assembly. If these dimensions were modified in the future, i.e. if different vertical support beams are used, the stoppers may need to be redesigned.

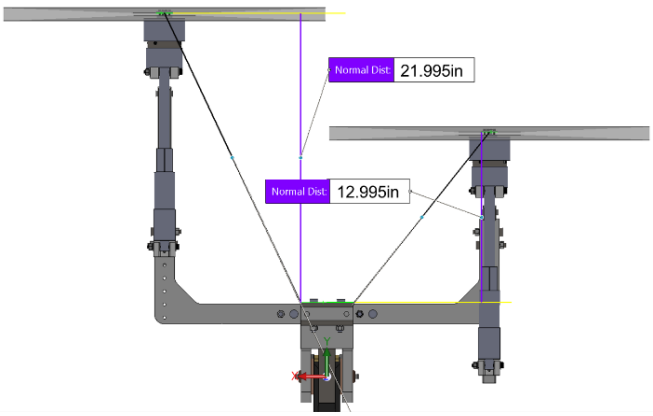

Figure 10: Front view of rotor assemblies, at minimum height of 13 inches and maximum height of 22 inches.

Rotor Assembly

Going from top to bottom, the rotor assembly consists of the following: the rotor cover, rotor, rotor motor, motor-load cell interface, load cell, clevis interface, hinge, flanged bearings, dowel pin, shoulder bolts, thrust bearings, linear actuator, bottom clevis, locknuts, and screws (see Figures 11, 12, and 13). The dowel pin is press fit into the flanged bearings and the hinge, ensuring the bearings take all the rotation. The flanged bearings are press fit into the vertical support beam. The dowel pin is the point of rotation for the rotor.

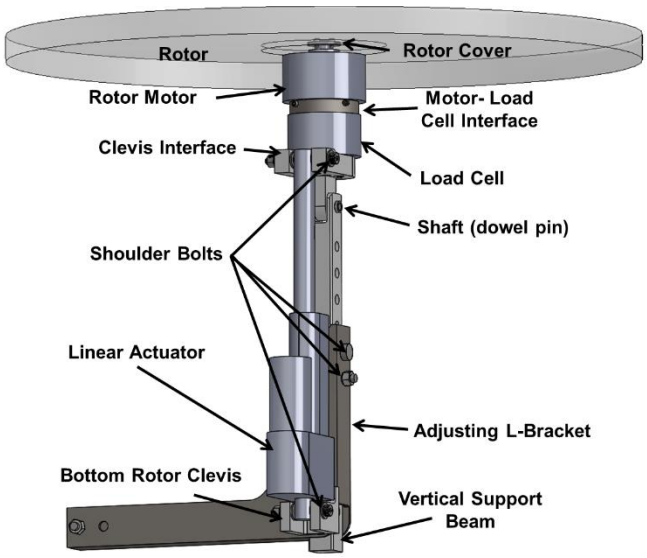

Figure 11: View of Rotor Assembly.

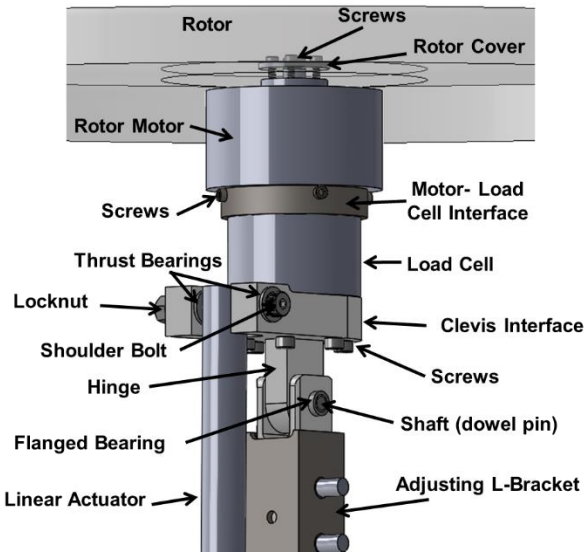

Figure 12: Close up view of the top of the rotor assembly.

The clevis interface is connected to the load cell via screws coming in from the bottom. A shoulder bolt goes through the clevis interface and the hole in the top of the linear actuator. It is then secured by a locknut on the other side. This shoulder bolt is the point of rotation for the top part of the linear actuator. There are thrust bearings in between each of the parts to provide a smooth surface against which the parts can rotate. As the linear actuator moves up and down, it pulls and pushes the clevis interface, causing the rotor assembly to rotate about the dowel pin.

Figure 13: MTB Rotor Assembly in wind tunnel.

The bottom rotor clevis holds the bottom of the linear actuator to the vertical support beam (see Figure 11 and 14). Note that the bottom rotor clevis is connected to the vertical support beam, and not the adjusting L-bracket. This is because the point of rotation (dowel pin) for the rotor is about the top of the vertical support beam. It is essential that the placement of the linear actuator on the vertical support beam is maintained. This positioning has been designed to ensure maximum range of motion. The bottom rotor clevis is secured to the vertical support beam via two screws, and there are access holes along the back of the adjusting L-bracket for ease of assembly (see Figure 9). The method for securing the linear actuator to the bottom rotor clevis is the same as that of the clevis interface (using shoulder bolt, thrust bearings, and a locknut).

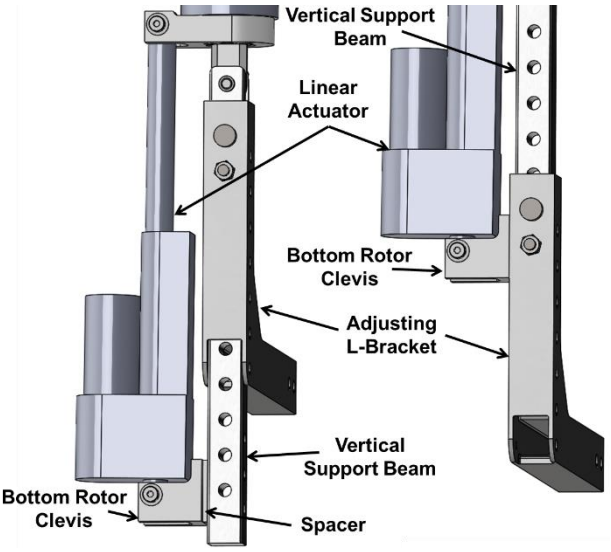

Figure 14: Close up, side view of bottom of rotor assembly in short (left) and tall (right) configurations.

The clevis moves with the beam to maintain the same vertical distance so the actuator can function properly. It is also important for the horizontal distance to be maintained in order to maintain the kinematics of the tilting mechanism at all vertical rotor positions. In the taller configurations, the bottom rotor clevis rests against the vertical adjusting beam, but in the shorter configurations, there is a 0.125 inch gap. This gap is filled with a spacer shown in Figure 14. This spacer maintains the bottom rotor clevis in the proper position as well as provides enough surface contact for a strong connection.

Returning to the top of the rotor assembly, the hinge is connected to the clevis interface. The top of the clevis interface has countersunk holes which line up with holes on the top of the hinge, see Figure 12.

The manufacturer of the load cell refers to the "metric side" as the top side, and the "non-metric side" as the bottom side (mounting to the hinge). The motor-load cell interface is connected to the load cell and the rotor motor. There are two interfaces used to do this. The top interface slides into the bottom interface, and they are connected together via screws through the holes on the outside (shown in Figure 15). The holes on the inside of the interface align with holes on the rotor motor and the load cell. These holes are countersunk so that the parts lie flat. The cutout in each piece is for the RPM sensor. The top piece has two tapped holes which secure a bent piece of sheet metal that holds the sensor (see Figure 16).

Figure 15: Exploded View of Motor – Load Cell Interface Assembly.

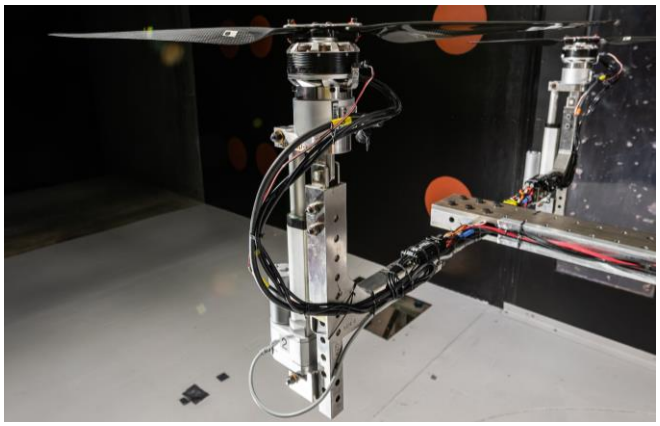

Figure 16: Picture of back of MTB Rotor Assembly in tunnel.

The rotor itself has a hole pattern that corresponds to the mounting holes on the top of the outrunner motor. Screws are used to secure the rotor to the motor and torque stripe is used on the screw heads to indicate any loosening of the screws. The rotor can be removed and replaced with a different rotor if the corresponding mounting holes have the same pattern. Otherwise, a new motor-load cell interface may be required. Each motor is individually controlled via a servo controller and LabVIEW feedback control system. All manufactured parts of this assembly were from 17-4 except for the inside motor-load cell interface, which was made out of 13-8PH H950, so no galling can occur.

Installation Assembly

The bridge crane in the wind tunnel facility was used to move the assembly in and out of the tunnel. The strut assembly was installed first, and then the strongback assembly was placed on top and secured into place. Next the L-brackets were installed, and then the rotor assemblies were assembled.

The strut was secured to the mounting block via large screws, see Figure 17. Inside the strut is a jackscrew which can be turned with a square shaft through the bottom of the strut. The gearbox-strut interface, see Figure 18, fits into the bottom of the strut and slides over the gearbox. The gearbox is secured to the mounting block via screws counterbored into the top of the mounting block. The motor-gearbox interface holds the gearbox and the stepper motor together. The stepper-gearbox bushing slides on top of the shaft of the stepper motor and is secured to the gearbox via the gearbox's shaft collar. This assembly allows the stepper motor to turn the jackscrew inside of the strut, thus moving the lug (ear) up and down and pitching the MTB assembly inside the tunnel.

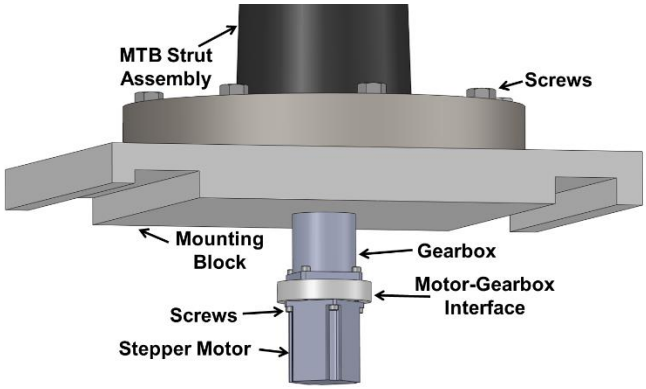

Figure 17: Bottom View of Installation Assembly.

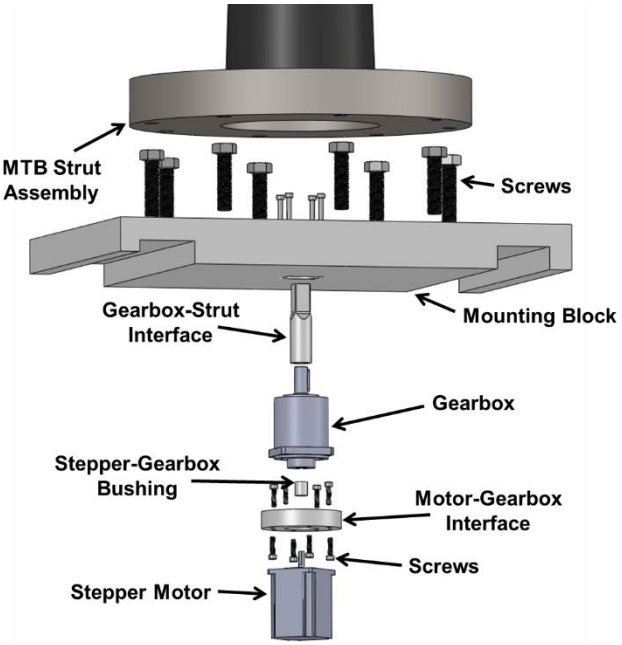

Figure 18: Exploded view of Installation Assembly.

LOAD AND STRESS ANALYSIS

This section describes the types of analyses done, the method by which the analyses were performed, and presents a summary of the results. Analysis was performed on each component in the Strut Assembly, Beam Assembly, and the Rotor Assembly. A Blade Out Analysis was also performed on essential parts. Finite Element Analysis, FEA, was performed using SolidWorks. Additional calculations were done to estimate the loads that various components of the system would experience. The estimated maximum thrust of each rotor was 30 lb, with an estimated maximum in plane load of +/- 20 lb. For the analysis however, the maximum in plane load was eventually set to +/- 26.5 lb. This was the largest in plane load that all of the components could handle while still maintaining safety factors greater than 5 on yield strength. This +/- 26.5 lb load was used in the safety of flight loads monitoring. The off the shelf components were also analyzed. For the full detailed load and stress analysis of the MTB, see Ref. 6.

The positions of the rotors are often referred to as being in "helicopter mode" or "airplane mode." Helicopter mode refers to when the rotors are straight up and have 0 deg rotation, similar to a helicopter operating in a vertical flight maneuver. Airplane mode refers to when the rotors are tilted the full 90 deg forward and produce a thrust going forwards, similar to an airplane in horizontal flight. It should also be noted that pitch refers to the rotation of the strongback about the shaft that goes through the strut and tilt refers to the rotation of the rotors about the dowel pin in the top of the vertical support beam.

Finite Element Analysis

FEA was performed in SolidWorks on each MTB assembly to predict the maximum stress and the maximum deflection in various configurations. The maximum allowable angular deflection was set to 0.1 deg, in order to obtain accurate data. For this reason, many of the parts have high safety factors, and are over designed with respect to loads and stress. To find the maximum allowable deflection of the strongback, the length of the strongback, 80.625 inches, was divided by 2 and multiplied by the sine of 0.1 deg to give the maximum vertical deflection allowed, 0.07036 inches. For several of the FEA studies done on assemblies, the whole assembly was saved as a part file in order to minimize the run time and complexity of each study. This could make the study less accurate, since the assembly was now treated as a part in Solidworks. However, different components could still be selected within the part file and given different material properties.

When performing FEA in Solidworks, each part was constrained in a way that mimicked its relationship to the other components. Loads were solved for and then applied along the corresponding surfaces. The material properties used in the FEA are given in Tables 3 – 6 in the Appendix. In some cases, the mesh had to be refined several times before the stress converged. Sometimes the constraints were applied in a way that yielded stress singularities. This was resolved by modifying the constraints or modifying the part, often by smoothing the geometry of the part (e.g. applying small fillets). If the simulated part was modified at all, care was taken to ensure that the manufactured part reasonably matched the modified part.

Derivations

A number of specific loads were derived from free body diagrams and used in the finite element analyses. This section describes the method that was used to calculate these loads.

From a structural integrity perspective, the main areas of concern for the Strut Assembly were the forces going through the pitching mechanism (threaded rod, lug, clevises, and bearings) and the forces on the upstream and downstream stopper. These three forces were derived and calculated in their respective worst-case scenarios. These forces were then used in the stress analyses and for the FEA of the different parts of the Strut Assembly. Calculation 1 derives the force that goes through the pitching mechanism. Calculation 2 derives the maximum force on the upstream stopper. Calculation 3 derives the maximum force on the downstream stopper. Calculation 4 derives the force that goes through the linear actuator, which is part of the Rotor Assembly.

Calculation 1: Force through the Pitching Mechanism

The diagram of the strut assembly in Figure 19 shows the axial force going through the pitching mechanism F_{a_s}, the weight of the assembly F_G, the vertical force required to move the lug F_{ay}, and the various dimensions. The angle α represents the angle of the axial force going through the pitching mechanism with respect to the horizontal axis. The angle θ represents the rotation of the strongback with respect to the vertical axis. The location of the center of mass of weight was found using the model in SolidWorks. F_p was the force from the rotors. Figure 19 shows the force from the rotors and the angle at which the rotors are rotated relative to their respective vertical axes, β.

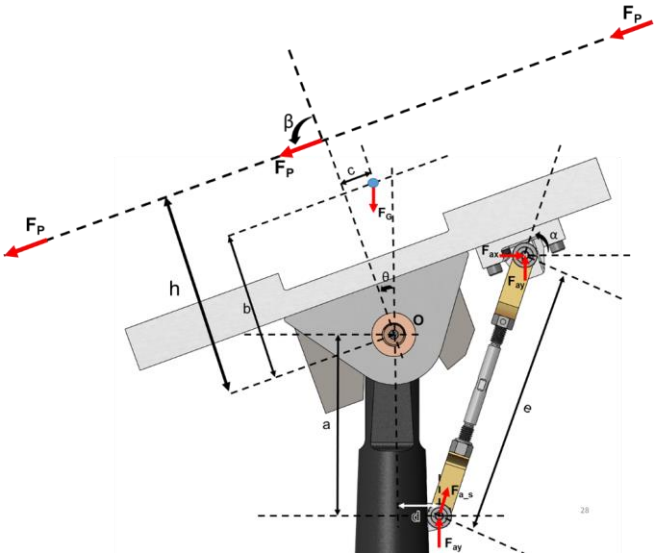

Figure 19: Schematic of Strut Assembly in 20 deg forward pitch configuration.

The sum of the moments about the origin (point O) was set to zero. The final equation solving for the axial force going through the pitching mechanism was:

$$F_{a_s} = \frac{6*F_P*h*sin\beta + F_G*(b*sin\theta - c*cos\theta)}{-a*cos\alpha - d*sin\alpha} \quad (1)$$

Equation 1 was used to solve for the axial force in various configurations. This equation was implemented for rotor tilt between 90 deg forward and 5 deg backward, in its standard configuration, as well as rotor tilt of 20 deg backward, when the bottom rotor clevis was secured to the top two holes of the vertical support beam.

There are several configurations for the MTB in which the blades come closer than 5 inches to the walls. There are also configurations in which the MTB can theoretically operate at a 30 lb thrust load. For example, the rotors are planned to have only 10 lb of thrust in airplane mode. Although there are no plans to operate the MTB in these problematic configurations, the loads for these configurations were calculated. These loads are referred to herein as theoretical loads. The maximum operational loads and maximum theoretical loads were found for different tilt angles of the rotors and pitch angles of the strongback.

The overall maximum operational load case was for a rotor tilt of 45 deg forward, in its short configuration, when the strongback was pitched 20 deg forward. The overall max operational load was 657 lb. The overall max theoretical load case was for a rotor tilt of 90 deg forward, in its tall configuration, when the strongback was pitched 30 deg forward. The overall max theoretical load was 1453 lb.

Calculation 2: Force on the Upstream Hard Stop

In this section, the maximum potential force that will go through the upstream hard stop was calculated. The purpose of the upstream hard stop was to stop the MTB from rotating forward in the event that the tilting mechanism (the threaded rod, clevises, etc.) failed. The hard stop was positioned to hit the strut when the MTB was 22 deg forward. The worst-case scenario that would result in the maximum load on the hard stop was when all the rotors were in the tall position, tilted 90 deg forward, with 30 lb of thrust. During testing, when the rotors are tilted 90 deg forward, the thrust for each rotor was planned to be less than 10 lb. Therefore, this worst loading case is a theoretical loading case.

F_{w_p} was the weight of two of the rotor assemblies and one lateral support beam. F_p was the thrust from the rotor. F_{w_s} was the weight of the strongback assembly and the top of the strut assembly (hinges and supporting interfaces). The location of the center of mass of the different weights were found using the model in SolidWorks.

The MTB is rotated forward 22 deg, as shown in Figures 20 and 21. Note that some similar variables were used in Calculation 1, but they may have different values in Calculation 2. Figure 21 shows a zoomed in view of the schematics about the center of rotation. This figure shows the force F_{a_Uhs} which is the force on the upstream hard stop. Using these schematics, this force was derived and calculated.

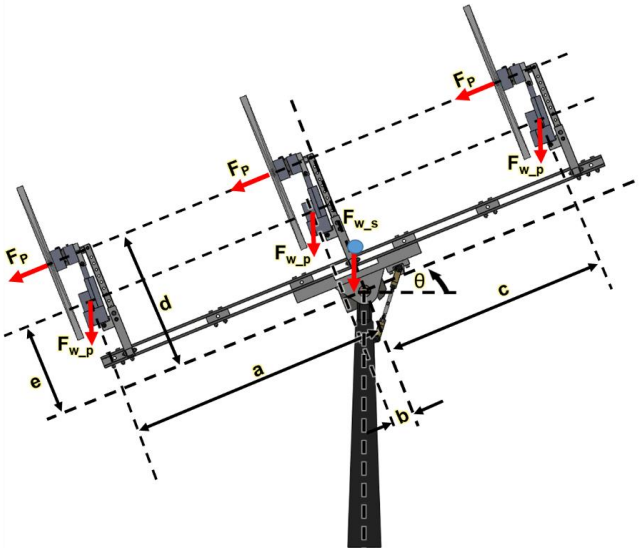

Figure 20: Schematic of MTB with 22 deg pitch and 90 deg tilt – Calculation 2

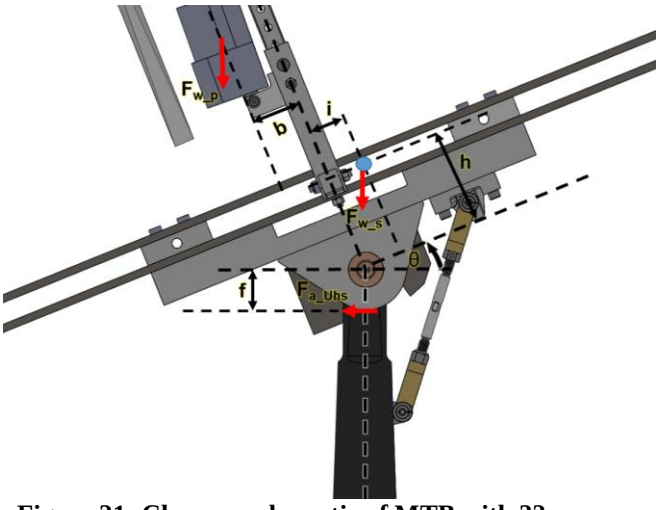

Figure 21: Close up schematic of MTB with 22 deg pitch and 90 tilt – Calculation 2

The sum of the moments about the center shaft (point of rotation) was set to zero.

$$F_{a_{Uhs}} = (F_{w_p} * (\cos\theta * (a + b - c) + 3 * e * \sin\theta) + 6 * F_P * d + F_{w_s} * (-i * \cos\theta + h * \sin\theta)) * \frac{1}{f} \quad (2)$$

The force going through the upstream hard stop, F_{a_Uhs} was calculated to be 2254.6 lb. This force was used in the FEA of the upstream hard stop.

Calculation 3: Force on the Downstream Hard Stop

In this section, the maximum potential force that will go through the downstream hard stop was calculated. The method for deriving Calculation 3 was very similar to that of Calculation 2. The hard stop was positioned to hit the single heavy strut when the MTB was 14.25 deg backward. The worst case scenario that would result in the maximum load on the hard stop was when all the rotors were in the tall position, rotated 20 deg backward, with 30lbs of thrust. Note that in order for the rotor to rotate 20 deg backward, the bottom rotor clevis needed to be moved to the top 2 holes in the vertical support beam. This worst loading case is a theoretical loading case, see schematic of model in Figure 22.

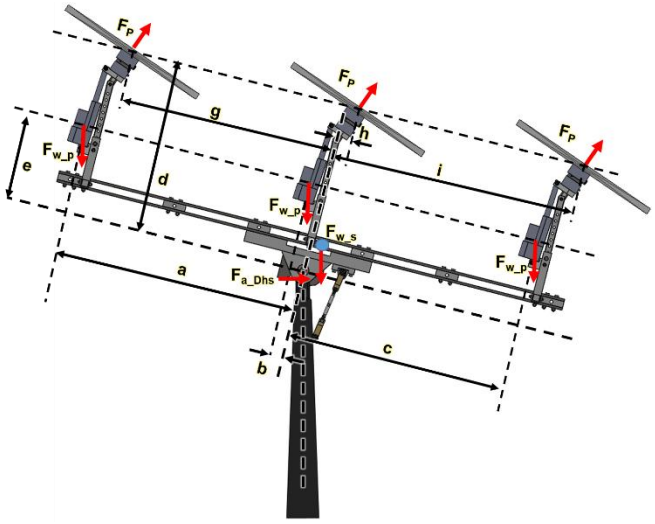

Figure 22: Schematic of MTB with -14.25 deg pitch and -20 deg tilt – Calculation 3

The variables F_{w_p}, F_p, and F_{w_s} have the same definition as in Calculation 2. Note that the other variables are similar to Calculation 1 and 2, but they may have different values in Calculation 3. Figure 23 shows a zoomed in view of the schematics about the center of rotation. This figure shows the force F_{a_Dhs} which is the force on the upstream hard stop. Note that the angle θ, which represented the rotation of the strongback, was negative. θ was taken to be zero about the horizontal axis. Figure 24 shows a zoomed in view of the schematics of the rotor. Here, the angle α was also negative; however, 0 deg was defined at the vertical axis. Using these schematics, the force F_{a_Dhs} was derived and calculated.

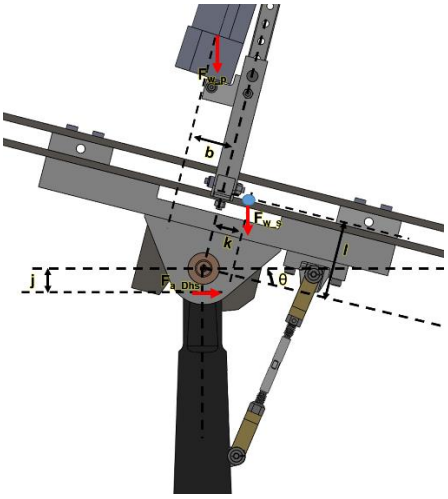

Figure 23: Close up schematics of MTB with -14.25 deg pitch and -20 tilt, view of pitching mechanism.

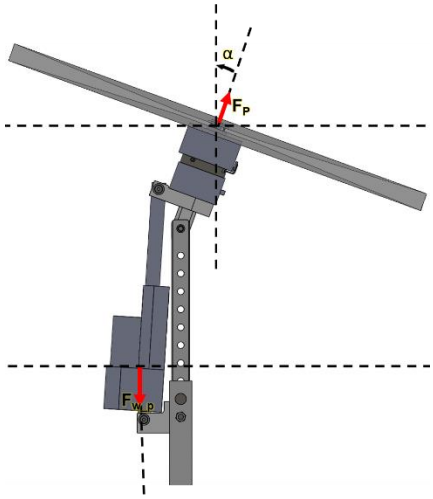

Figure 24: Close up schematics of MTB with -14.25 deg pitch and -20 tilt, view of rotor.

The sum of the moments about the center shaft (point of rotation) was set to zero.

$$F_{a_{Dhs}} = \left(-F_{w_p} * (\cos\theta * (a + b - c) + 3 * e * \sin\theta) - 6 * F_P * \sin\alpha * d - 2 * F_P * \cos\alpha * (-g + i + h) - F_{w_s} * (-k * \cos\theta + l * \sin\theta)\right) * \frac{1}{j} \quad (3)$$

The force going through the downstream hard stop, $F_{a_{Dhs}}$ was calculated to be 2816.6 lb. This force was used in the FEA of the downstream hard stop.

Calculation 4:

The schematic in Figure 25 shows the forces acting on the rotor. The angle θ represents the rotation of the rotor about point O with respect to the vertical axis. F_{w_p} is the weight of the rotor assembly above point O. Note that this weight is different than previous weights of the rotor assembly. F_{pp} is the in-plane load of the rotor. The thrust of the rotor is directly in line with the point of rotation, so it cancels out when

solving for the moment. F_{a_L} is the axial force through the linear actuator. The angle α is the rotation of the axial force (or the linear actuator) about the horizontal axis.

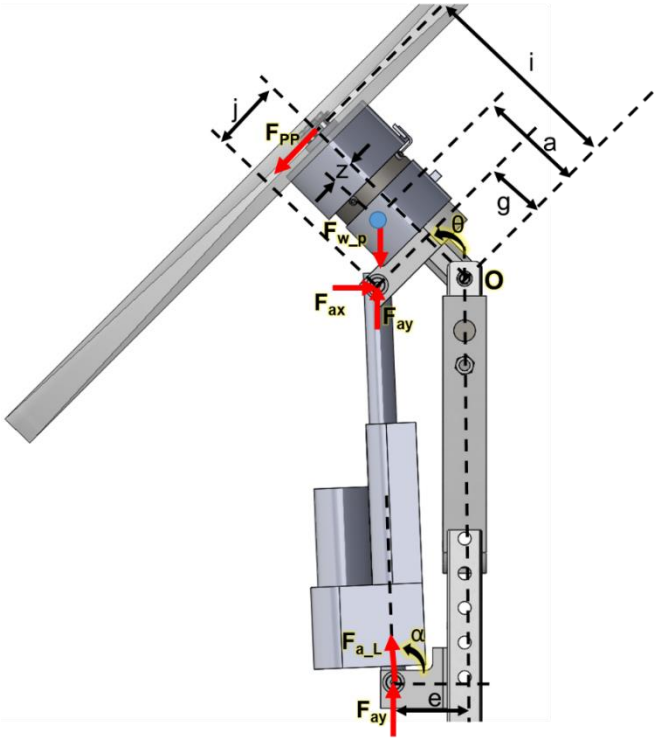

Figure 25: Schematic of rotor assembly – Calculation 4.

The sum of the moments about the point of rotation, O, was set to zero and the axial force through the linear actuator was solved for.

$$F_{a\_L} = \frac{(F_{w\_p} * a * \sin\theta + z * \cos\theta) + (F_{PP} * i)}{(\sin\alpha * (j * \cos\theta + g * \sin\theta)) + (\cos\alpha * (g * \cos\theta - j * \sin\theta))} \quad (4)$$

The axial force was calculated for different configurations of rotor tilt. It should be noted that the rotation of the strongback was assumed to be zero. The maximum axial force going through the linear actuator occurred at rotor tilt angles of 90 deg forwards and 20 deg backwards, and it was about 110 lb for both configurations.

Hand Calculations

A thread pullout calculation was performed for some of the screws and the threaded rod. The equation used is shown below.

$$P = \frac{1}{3}\pi d_m F_s L \quad (5)$$

Where P is the pullout load, d_m is the mean diameter or pitch diameter of the threads, F_s is the material ultimate or yield stress, and L is the length of the thread engagement [Ref. 7]. The safety factor (SF) was calculated by dividing the calculated maximum pullout load by the expected load.

A shear tearout calculation was performed on some of the clevises in the assembly.

$$A_{shear} = A_s = 2t(e - \frac{d}{2}) \quad (6)$$

Where A_s is the shear area, t is the thickness of the clevis, e is the distance from the edge to the center of the hole, and d is the diameter of the hole. After finding the shear area, the shear stress could be calculated using Equation 7.

$$\sigma_s = \frac{F/2}{A_s} \quad (7)$$

The maximum shear stress, or AISC Allowable Shear Stress, was found by multiplying the yield strength of the material by 0.4. The SF could then be calculated by dividing the maximum shear stress by the calculated shear stress.

A shear tearout from bending calculation was performed on some of the shoulder screws in the assembly using Equation 8.

$$Max\ Bending\ Moment = M_{max} = \frac{P}{2}\left(a + \frac{l}{4}\right) \quad (8)$$

Where P was the maximum load, a was half of the clevis thickness, and l was the distance between the clevis arms. The stress due to bending was then calculated using Equation 9.

$$\sigma_B = \frac{Mc}{I} \quad \text{where,} \quad I = \frac{1}{64}\pi D^4 \quad (9)$$

The rated shear strength was then divided by the calculated shear stress due to bending to give the SF.

Blade Out

Blade out is the case in which one of the rotor blades suddenly comes off of the rotor due to a failure at or near the blade root. The single remaining blade would continue to rotate until power was cutoff, but the single rotating blade would generate a large rotating force. This force was derived using the center of mass of the single blade at specific speeds. This force would be in the plane of the rotor. At 4000 RPM the max alternating in plane load would be 142 lb. At 6000 RPM the max alternating in plane load would be 320 lb. Although the rotors should not be operating at speeds higher than 4000 RPM, they are individually capable of going up to 6000 RPM. Thus, the load used for the blade out analysis was the 320 lb alternating in plane load. Because this situation is not a normal operating condition, the analysis only needs to show a SF of greater than 1.0 on yield strength. Deflection is not considered in these studies. A refined mesh was used on these studies to ensure accurate results. Of all of the blade out scenarios, the worst cases were when the rotors were in helicopter mode with the load going backward, and with the rotors in airplane mode with the load going downward. All of the blade out scenarios gave SFs greater than 1.0.

Results

Table 2 shows a summary of the safety factors of all the components in the MTB. The SF is noted "conservative" when the SFs were calculated using McMaster specified maximum loads/stresses. It is expected that McMaster included a SF in these numbers as well. An asterisk, " * ", notes that this SF was obtained from the maximum theoretical

load, and that the MTB is not planned to operate in that configuration. It should be noted that a SF of 4 on ultimate strength and a SF of 3 on yield strength is required for testing in the wind tunnel. It should also be noted that all parts that have a SF of at least 5 on yield do not need to have a fatigue analysis performed. This is why fatigue was not considered in this study.

Table 2: Safety Factor Summary

PART	MATERIAL	MAX STRESS/LOAD	SF YIELD	SF ULTIMATE
Strongback Assembly	17-4/13-8	5.17 ksi	35.78	
Strut Support Interface	17-4	2.33 ksi	79.4	
Upstream Hard Stop	17-4	20.20 ksi	9.25	
Downstream Hard Stop	17-4	29.62 ksi	6.25	
Strut Assembly - Designed Lug	17-4	5.21 ksi	35.5	
Bottom Clevis - Pitching Mechanism	4130	1418 lb	12.43	
Top Clevis - Pitching Mechanism	4130	1418 lb	12.49	
Large Hinge	17-4	0.66 ksi	280	
Flanged Sleeve Bearing	954 Al-Brz	726.5 lb		*1.45 (conservative)
Dowel Pin – Pitching Mechanism	416 SS	1453 lb		7.57 (conservative)
Screw – Strut Assembly (for lug)	Alloy Steel	726.5 lb		13.8 (conservative)
Ball Bearing	Steel	210 lb		*4.76 (conservative)
Dowel Pin – Strut Assembly	416 SS	420 lb		107 (conservative)
Threaded Rod	17-4	1453 lb	18.3	
Adjusting L-Bracket	17-4	15.49 ksi	7.67+	
Vertical Support Beam	13-8	26.03 ksi	5	
Lateral Support Beam	13-8	5.444 ksi	31	
Clevis Interface - Rotor Assembly	17-4	7.73 ksi	23.92	
Bottom Clevis - Rotor Assembly	17-4	2.63 ksi	70.4	
Linear Actuator		110 lb	5	
Rotor-linear actuator – bearing	Steel	55 lb	10.9	
Flanged Sleeve bearing – Rotor	863 Brz	12.75 lb	32	
Shoulder Screw - Rotor Bottom	Alloy Steel	110 lb		11.3 (conservative)
Shoulder Screw - Rotor Top	Alloy Steel	110 lb		8.6 (conservative)

CONCLUSION

The MTB was designed, manufactured, assembled, and then tested in the U.S Army's 7-by 10-Foot Wind Tunnel at NASA Ames Research Center. Prior to testing, a detailed analysis was performed on the MTB and its components, to ensure that it would be able to withstand the loads during testing, as well as take accurate measurements. The MTB has been tested in different rotor configurations and has shown that it can be operated safely and effectively in the wind tunnel. There are future plans for the MTB to continue testing in the 7- by 10-Foot Wind Tunnel, and the MTB also has the potential to be tested in larger facilities like the 40- by 80-Foot or 80- by 120-Foot Wind Tunnels at NASA Ames.

ACKNOWLEDGEMENTS

The authors would like to thank the following people for their contributions to this project. Gina Willink, lead of the Ames Aeromechanics Mechanical Systems Team, helped throughout the design process, reviewed the design and analysis, and provided invaluable advice. The NASA Machine Shop Team, led by Robert Kornienko and Vincent Derilo, machined the parts of the MTB and provided guidance and helpful suggestions during the design process. Steve Nance along with the other members of the 7- by 10-Foot Wind Tunnel test crew were critical to the project's success. Finally thank you to William Warmbrodt for his continued outstanding leadership.

REFERENCES

[1] C. Russell, G. Willink, Theodore, C, and B. Glasner, "Wind Tunnel and Hover Performance Test Results for Multicopter UAS Vehicles." NASA/TM—2018-219758, February, 2018.

[2] C. Russell and et al, "Multicopter UAS Performance Test 2." NASA/TM—TBD.

[3] G. Cheng, G. Nunez, C. Russell, M. Avera, and J. Dorrerweich, "Wind Tunnel Test Results for an Overlapped Quadrotor Configured UAS," presented at the AHS International 74th Annual Forum and Technology Display, Phoenix, AZ, May 14-17, 2018.

[4] S. Conley and C. Russell, "Comparing CFD Predictions of the Multirotor Test Bed with Experimental Results," presented at the Abstract accepted to VFS 76th Annual

Forum and Technology Display, Montréal, QC, Canada, May 19-21, 2020.
[5] C. Russell and S. Conley, "The Multirotor Test Bed – A New NASA Test Capability for Advanced VTOL Rotorcraft Configurations," presented at the Abstract accepted to VFS 76th Annual Forum and Technology Display, Montréal, QC, Canada, May 19-21, 2020.
[6] S. Conley, "Load and Stress Analysis of the Multirotor Test Bed." NASA/TM – TBD.
[7] R. T. Barrett, "Fastener Design Manual," Mar. 1990.
[8] Barrett, "17-4 PH Stainless Steel Product Data Bulletin." AK Steel, https://www.aksteel.com/sites/default/files/2018-01/174ph201706.pdf.
[9] "Aerospace Material Specification AMS5629." SAE International, Aug-2016.
[10] "Brass and Bronze Standard Casting Alloys Chart of Specifications Aerospace Material Specification AMS5629," https://www.nationalbronze.com/pdfs/spec_reference.pdf.

APPENDIX

Table 3: Material Properties of 17-4PH H900 Stainless Steel [8].

17-4 PH H900	Value	Units
Elastic Modulus	2.85E+10	psi
Poisson's Ratio	0.272	N/A
Shear Modulus	11000000	psi
Mass Density	0.282	lb/in^3
Tensile Strength	200000	psi
Yield Strength	185000	psi
Thermal Expansion (-100 to 70ºC)	5.80E-06	in/in/ºF

Table 4: Material Properties of AISI 4130 Heat Treated to 180 ksi.

AISI 4130 Steel Heat Treated	Value	Units
Elastic Modulus	2.97E+07	psi
Poisson's Ratio	0.285	N/A
Shear Modulus	11603019.01	psi
Mass Density	0.283599162	lb/in^3
Tensile Strength	180000	psi
Yield Strength	160000	psi
Thermal Expansion (-100 to 70ºC)	7.00E-06	in/in/ºF

Table 5: Material Properties of 13-8PH H950 Stainless Steel [9].

13-8PH H950	Value	Units
Elastic Modulus	3.21E+07	psi
Poisson's Ratio	0.272	N/A
Shear Modulus	11100000	psi
Mass Density	0.282	lb/in^3
Tensile Strength	220000	psi
Yield Strength	205000	psi
Thermal Expansion (-100 to 70ºC)	5.90E-06	in/in/ºF

Table 6: Material Properties of 932 Bearing Bronze [10].

932 Bearing Bronze	Value	Units
Elastic Modulus	1.45E+07	psi
Poisson's Ratio	0.394	N/A
Shear Modulus	46252	psi
Mass Density	0.322	lb/in^3
Tensile Strength	35000	psi
Yield Strength	20000	psi
Thermal Expansion (-100 to 70ºC)	-	in/in/ºF